China Petroleum Processing and Petrochemical Technology

Catalyst Research Volume 23, Issue 2, November 2023 Pp. 3452-3466

STUDIES ON STRUCTURAL, PERMEABILITY AND DIELECTRIC PROPERTIES OF CU^{2+} SUBSTITUTED NI-ZN FERRITES

***M. K. Raju[1], M. Ratna Raju[2], K. Rajkumar[3], P. S. V. Shanmukhi[4], Shaik Jesus Mercy[8], P. Himakar[5], B. Srinivasa Rao[8], Praveen Choppara[6], B. Suryanarayana[7], K. Samatha[8]**

[1]Wellfare Institute of Science, Technology, and Management, Visakhapatnam - 531173, India

[2]Department of Physics (BS&H), Vignan's Institute of Information Technology, Duvvada, Visakhapatnam, A. P., India.

[3]Department of Engineering Chemistry, AUCE (A), Andhra University, India

[4]Department of Physics, Aditya College of Engineering and Technology, Surampalem, India.

[5]Department of Physics, P. R. Degree College (A), Kakinada-533001, A. P., India.

[6]Department of Chemistry, P. R. Degree College (A), Kakinada-533001, A. P., India.

[7]Department of Physics, Raghu Engineering College (A), Dakamarri, Bheemunipatnam Mandal, Visakhapatnam, A.P., India.

[8]Department of Physics, Andhra University, Visakhapatnam - 530003, India

Corresponding author: * E-mail: kalyanrs09@gmail.com (**M. K. Raju**)

Abstract: Cu^{2+} modified Ni-Zn ferrite samples through the chemical formula, $Ni_{0.7-x}Cu_xZn_{0.3}Fe_2O_4$ (NiCuZn) with '*x*' variations of 0.0, 0.05, 0.10 0.15, 0.2, 0.25, 0.3, 0.35, 0.4, 0.45 and 0.50 have been fabricated using low temperature conventional solid-state route. These samples have been characterized by X-ray diffraction (XRD), Scanning Microscopy (SEM) with Energy Dispersive Spectra (EDS), Fourier Transform Inferred Spectroscopy (FT-IR), and dielectric constant and permeability studies. As analyzed by XRD, the structure of such synthesized materials was a single-phase spinel. Agglomerated small particles with stoichiometric proportions were obtained from SEM and EDS. Two absorption bands around 600 cm^{-1} and 400 cm^{-1} related to tetrahedral (A) and octahedral (B) interstitial sites by FTIR agree with the spinel lattice. Dielectric polarization procedures explain the behavior of a dielectric constant by various hopping mechanisms of the free charge carriers. This phenomenon involved two different mechanisms: the domain wall displacement and the spin rotation in the domains. The experimental dielectric studies disclose the decreasing trend for both dielectric constant and loss factor with the Cu substitution. All possible parameters are dependable for enhancing the magnetic quality identified and presented in this work. These are highly suitable for multi-layer ferrite chip inductor applications with a considerable enhancement in permeability.

Keywords: Ferrite; solid-state method; spinel structure; dielectric; permeability.

1. Introduction

NiCuZn ferrites widely used in electronic devices have led to a growing interest in low-temperature sintered ferrites doping with copper (Cu) due to their novel electromagnetic properties towards a specific application [1]. The multilayer ferrite chip inductors widely applied in devices like inductors, cores, converters, magnetic heads, electromagnetic wave absorbers, and multilayer chip inductors with high attenuation and wide bandwidth have been improvised as a high-performance electromagnetic interference (EMI) device [2-5]. These ferrite devices (nonreciprocal passive unit, which is irreplaceable for the telecommunication industry) are made with a co-fired, multilayer structure of ferrite chips, dielectric and internal conductors [6]. In these devices, a manufacturing process of the defective multilayer chip devices involves the capacitor, and inductor materials are co-firing because of their high frequency at low-firing temperature and increased permeability in the radiofrequency region (5Hz-20Hz). High permeability, high-quality factor, and increased resonating frequency are desirable characteristics for multilayer ferrite chip inductors [7, 8]. For achieving these properties, NiCuZn ferrite has been suitable for multi-layer chip inductors (MLCI) applications [9, 10]. The most important parameter for considering an application is initial permeability, which depends on a magnetic material's frequency. The daily soft magnetic materials are spinel nano ferrites. They can be tuned to more advanced materials with their proper doping. They have $M^{2+}Fe_2^{3+}O_4^{2-}$ the type of structure. M is the cation of transitional metal residing on their tetrahedral site and Fe^{3+} on the octahedral site [11]. NiZnCo ferrites can work efficiently at higher frequencies [12]. Higher resistivity and lower power loss are significant properties in several electronic devices [13]. Mallapur et al. and Knyazev et al. have investigated the structural, magnetic, and electrical properties of the spinel ferrite system of NiCuZn [14, 15]. There are many different ion-doped NiZnCu ferrites [16]. Among many preparation methods for synthesising nano ferrites like microemulsion, co-precipitation, ceramic, hydrothermal, sol-gel processes, etc., we have used the conventional ceramic method in our study [17].

In the current study, the structural, permeability and dielectric properties of $Ni_{0.7-x}Cu_xZn_{0.3}Fe_2O_4$ (x = 0.0, 0.05, 0.1, 0.15, 0.2, 0.25, 0.3, 0.35, 0.4, 0.45 and 0.5) ferrites were synthesised and investigated using XRD, SEM, FTIR, and LCR. Therefore, this study of initial permeability has greatly interested me in experimental ways. At this juncture, we report a high permeability value has been observed from less than 1100°C sintering temperature through a standard ceramic method.

2. Experimental Techniques

Ferrites with the composition of $Ni_{0.7-x}Cu_xZn_{0.3}Fe_2O_4$ (NiCuZn) samples were prepared by a conventional ceramic method. All chemicals used in this experiment are analytical reagent-grade chemicals. NiO, ZnO, CuO, and Fe_2O_3, the oxides were taken in the correct proportion and ground to a fine powder with methanol medium, mixing thoroughly for 6 hours using agate mortar and pestle. The powder was calcined for 4 hours at 850°C in a muffle furnace and cooled in the natural atmosphere. The calcined powder was crushed again for 2 hours with agate mortar and pestle. A binder like 5% Polyvinyl alcohol was added to press the pellets and toroid shapes. All the specimens were calcined at 1100°C for 4 hours in an air atmosphere.

Rigaku Miniflex II XRD was used for structural property, TESCAN, MIRA II LMH SEM for morphological and compositional study, FTIR for functional group separation and VSM for

Catalyst Research Volume 23, Issue 2, November 2023 Pp. 3452-3466

magnetic property characterization. The permeability and dielectric studies specimens were measured by using Hewlett Packard impudence Analyzer model 4192A. Complex permeability has been calculated as a frequency function up to 13 MHz at 298 K using a conventional technique to determine a circuit's complex impedance loaded with toroid-shaped ferrite samples.

3. Results and discussion

3.1 XRD Studies

The XRD plots for as formulated sampling and 800 ºC fired $Ni_{0.7-x}Cu_xZn_{0.3}Fe_2O_4$ (x = 0.0, 0.05, 0.1, 0.15, 0.2, 0.25, 0.3, 0.35, 0.4, 0.45 and 0.5) is shown in Figure 1. The sample structure is a cubic spinel structure in conformation as per JCPDS card No.48- 0489 [18]. The following equation is used to determine lattice constant 'a' [19]

$$\mathbf{a = d_{hkl}\sqrt{h^2 + k^2 + l^2}}$$

where d_{hkl} is the observed interplanar spacing, Bragg's law is used to calculate the d-spacing value and the lattice constant 'a'. Figure 2 depicts the lattice parameter 'a' control with the strength of the solution of replaced copper ion by NiCuZn magnetic oxides.

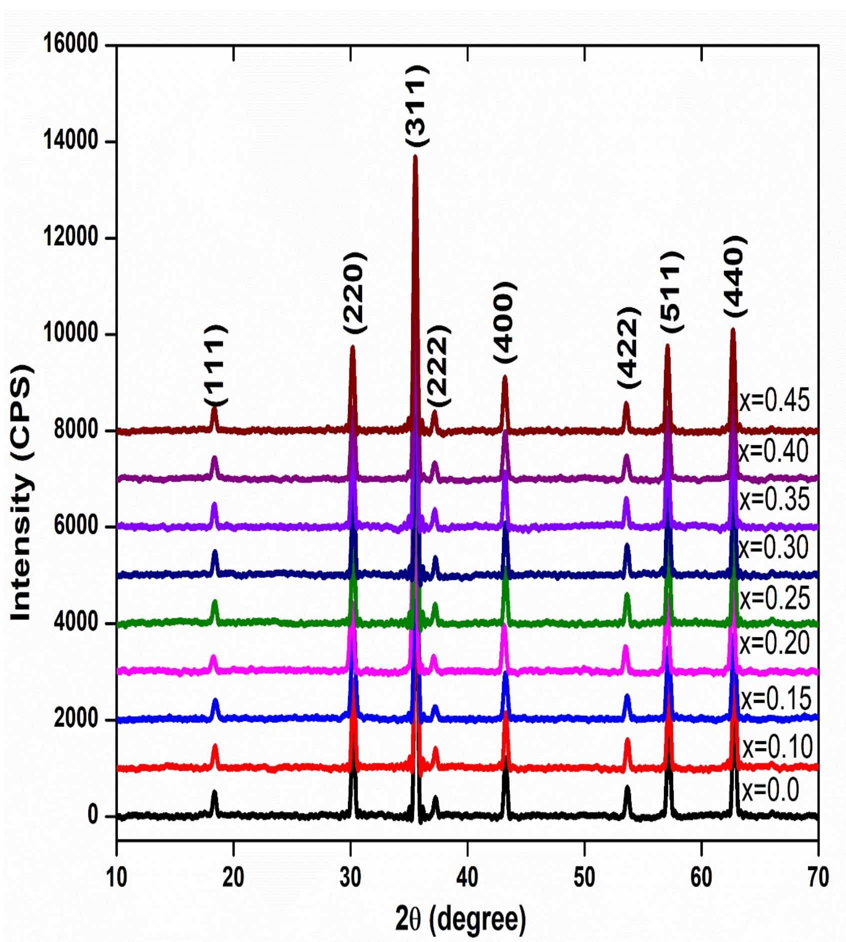

Figure 1: XRD patterns of $Ni_{0.7-x}Cu_xZn_{0.3}Fe_2O_4$ ferrites system

Catalyst Research Volume 23, Issue 2, November 2023 Pp. 3452-3466

The average crystallite size [20] is given by:

$$D_{311} = \frac{0.9\lambda}{\beta\cos\theta}$$

where λ, β and θ are X-ray's wavelength valued at 1.5406 Å, FWHM of (311) peaks and angle of diffraction, respectively.

The value of the lattice constant increases with Cu^{2+} content due to the larger ionic radii of Cu^{2+} (0.74 Å) ions than that of Zn^{2+} (0.72 Å)[21]. The lattice compression (Figure 2) may be due to the partial oxidation of Zn^{2+} to Zn^{3+}, Cu^{2+} to Cu^{3+}, and Zinc loss.

Table 1: Parameters of $Ni_{0.7-x}Cu_xZn_{0.3}Fe_2O_4$ ferrites system

Concentration (x)	Lattice constant a (Å)	Crystallite size (µm)	Space Group
0.0	8.3785	20.18	Fd-3m
0.05	8.3868	21.51	Fd-3m
0.1	8.3912	26.24	Fd-3m
0.15	8.3981	24.57	Fd-3m
0.2	8.4034	25.84	Fd-3m
0.25	8.4072	26.47	Fd-3m
0.3	8.4137	28.41	Fd-3m
0.35	8.4191	32.48	Fd-3m
0.4	8.4253	33.58	Fd-3m
0.45	8.4319	34.71	Fd-3m
0.5	8.4384	38.26	Fd-3m

As the particle's size decreases, the lattice constant variation is more significant. The diffraction peaks' wideness depicts the ferrite crystals' small size. The Scherrer method is used to find the average crystalline diameter of the powder sample. The studies saw that the crystallite sizes rise with increments in Cu^{2+} content, and the sizes are in the order of the micrometre range. As the sintering temperature enhances, the size of the particles also increases. Usually, sintering diminishes the lattice defects and strains, but it can cause a coalition of the crystallite, enhancing particle size [22]. Table 1 shows the lattice parameters and crystallite size values of the Cu-substituted NiZn ferrites system.

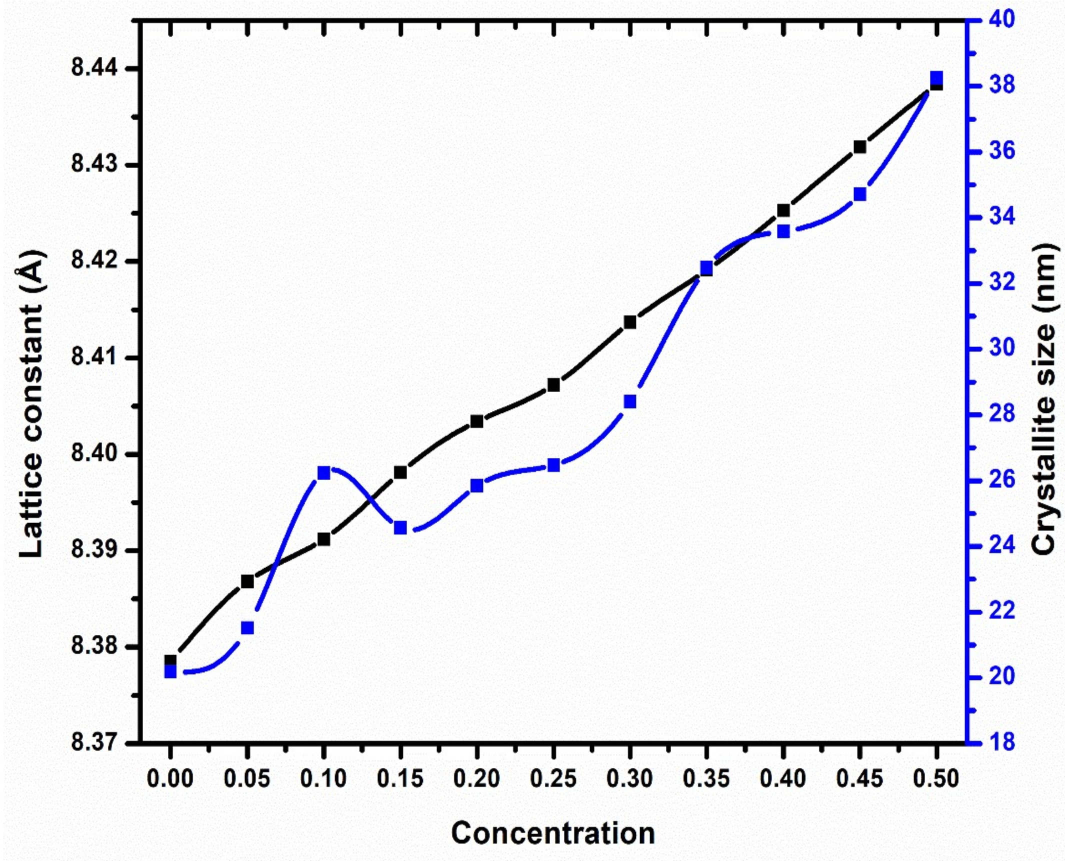

Figure 2: Lattice constant vs. crystallite size plot of $Ni_{0.7-x}Cu_xZn_{0.3}Fe_2O_4$ ferrites system

3. 2 Scanning Electron Microscope (SEM) studies

The considerable grain favours domain wall mobility, giving high permeability and low coercivity [18]. The SEM pictures of $Ni_{0.7-x}Cu_xZn_{0.3}Fe_2O_4$ (x = 0.0, 0.05, 0.1, 0.15, 0.2, 0.25, 0.3, 0.35, 0.4, 0.45 and 0.5) are shown from Figure 3, establish resembling a sphere-like microstructure with a prominent pore [23]. This indicates that nickel, copper, and zinc are non-miscible to each other. Figure 4 shows the EDS pattern of the samples for their elemental composition, where oxygen (O), copper (Cu), nickel (Ni), zinc (Zn), and iron (Fe) were found.

Catalyst Research Volume 23, Issue 2, November 2023 Pp. 3452-3466

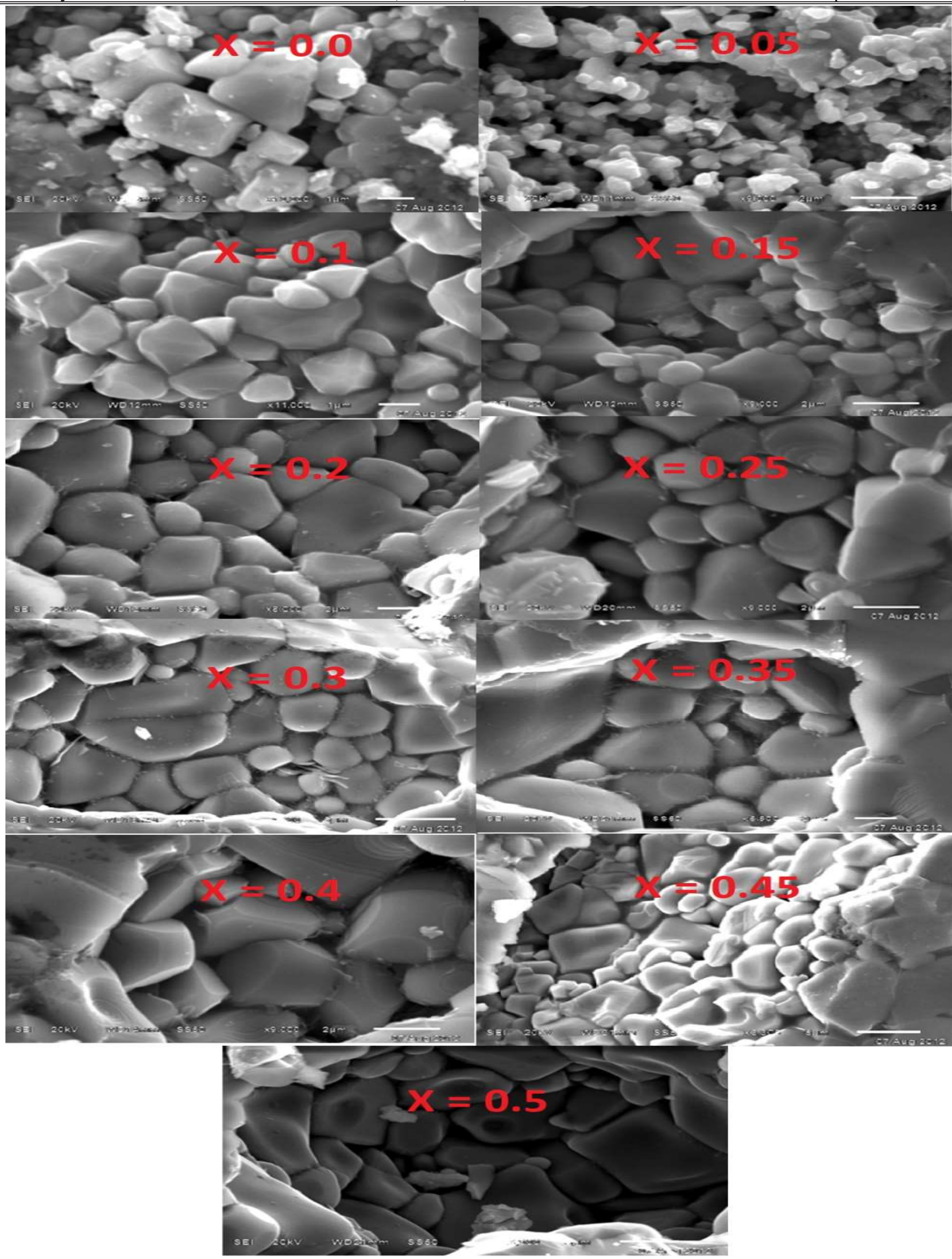

Figure 3: SEM images of $Ni_{0.7-x}Cu_xZn_{0.3}Fe_2O_4$ ferrites system

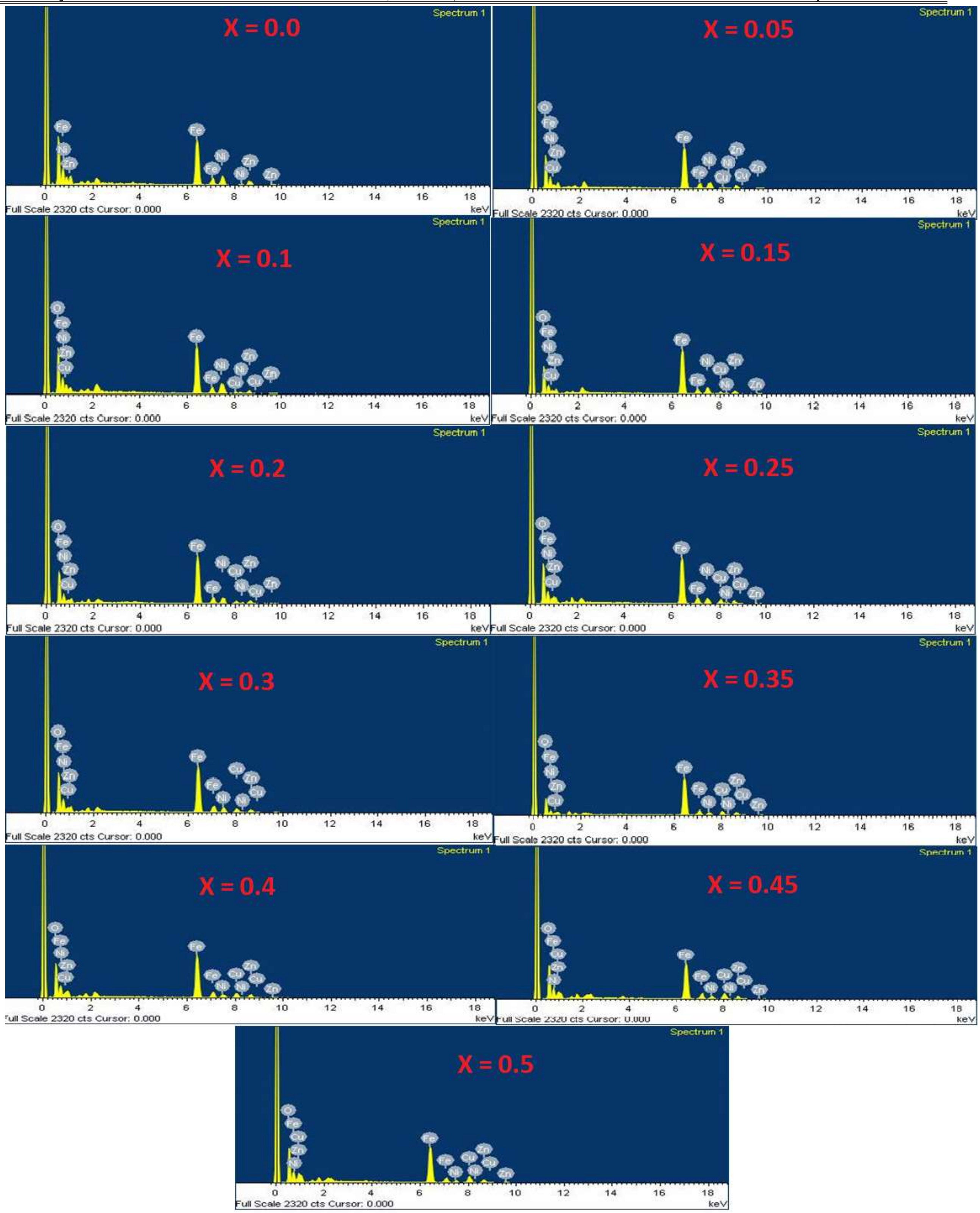

Figure 4: EDS spectra of $Ni_{0.7-x}Cu_xZn_{0.3}Fe_2O_4$ ferrites system

Catalyst Research Volume 23, Issue 2, November 2023 Pp. 3452-3466

3.3 FTIR studies

The compositional confirmation of the $Ni_{0.7-x}Cu_xZn_{0.3}Fe_2O_4$ (x = 0.0, 0.05, 0.1, 0.15, 0.2, 0.25, 0.3, 0.35, 0.4, 0.45 and 0.5) spinel ferrite was done based on FTIR spectra recorded in the interval 400 to 4000 cm^{-1} as shown in figure 5 and the values are listed in Table 2. The spinel ferrite (normal and inverse) can have four vibrational spectra activated by IR radiation. Three are from tetrahedral-octahedral molecules, and the fourth is from tetrahedral cation [24]. The two absorption bands around 605 cm^{-1} and 410 cm^{-1} show their spinel nature. The variation in bond length between Fe-O at tetrahedral and octahedral deviates the respective frequencies to their higher values. Their intensity increases with doping.

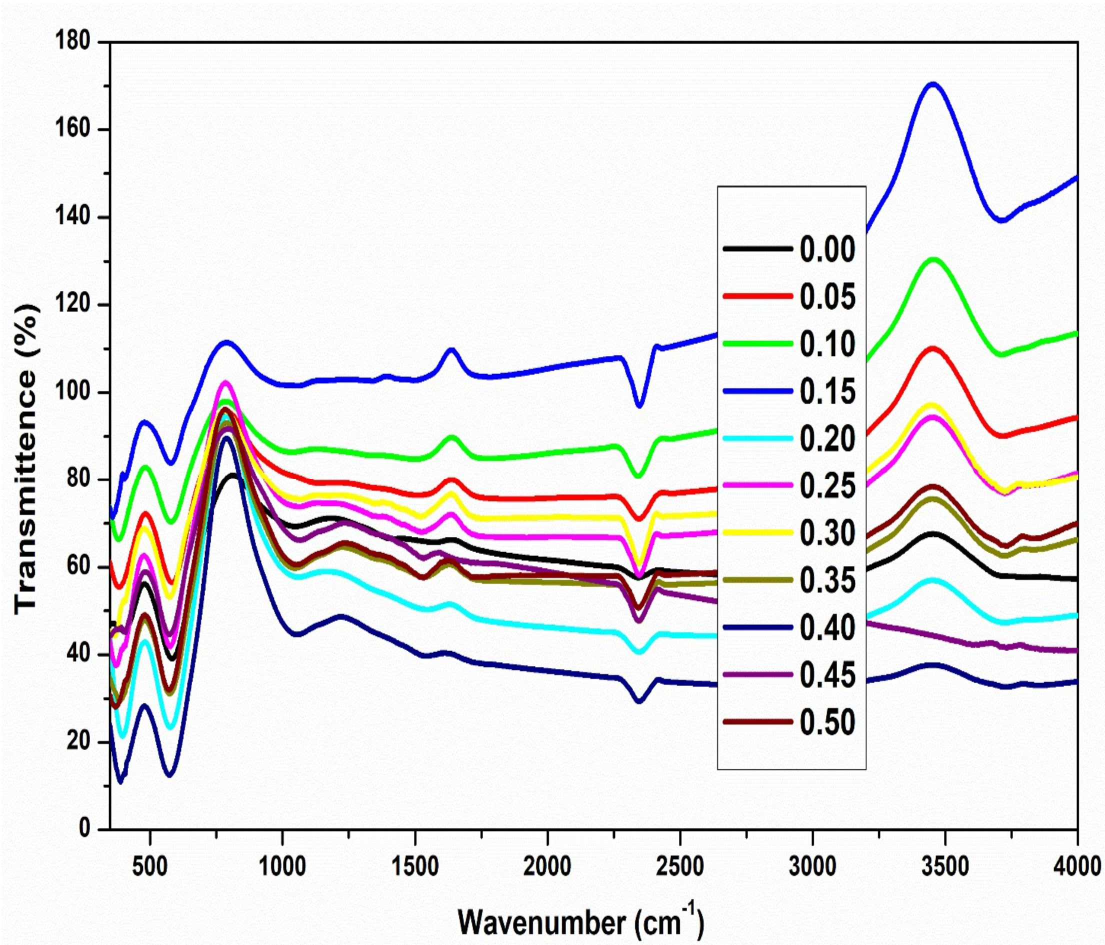

Figure 5: FTIR spectra of $Ni_{0.7-x}Cu_xZn_{0.3}Fe_2O_4$

Table 2: Bands of $Ni_{0.7-x}Cu_xZn_{0.3}Fe_2O_4$ ferrites system

Concentration (x)	$\vartheta 1$ (Cm^{-1})	$\vartheta 2$ (cm^{-1})
0.00	582.53	401.19
0.05	582.55	383.83
0.10	578.64	381.92

Catalyst Research Volume 23, Issue 2, November 2023 Pp. 3452-3466

0.15	**578.64**	**358.76**
0.20	**576.72**	**395.49**
0.25	**576.72**	**374.19**
0.30	**574.79**	**368.45**
0.35	**574.79**	**381.91**
0.40	**574.79**	**389.62**
0.45	**574.79**	**391.54**
0.50	**572.86**	**369.11**

3.4 Initial permeability

Figure 6 shows the decreasing of initial permeability with increasing doping copper concentration due to the diamagnetic behavior of copper, which decreases magnetic behavior up to saturation and leads to decreased initial permeability [25].

Complex permeability has been calculated as a frequency function up to 13 MHz at 298K for all the samples ($Ni_{0.7-x}Cu_xZn_{0.3}Fe_2O_4$ (x = 0.0, 0.05, 0.1, 0.15, 0.2, 0.25, 0.3, 0.35, 0.4, 0.45 and 0.5)). Plots between frequency and permeability (initial and complex) are shown in Figures 7 and 8. The values of initial permeability remain constant with increasing the frequency up to 10 MHz. This can be due to Bloch wall orientation, which is crucial in lower frequencies. The Bloch wall's direction is disturbed with a frequency, so the permeability rapidly decreases [26]. Beyond 10 MHz, the initial permeability rises, and resonance due to Bloch wall displacement is noticed and falls before 13 MHz.

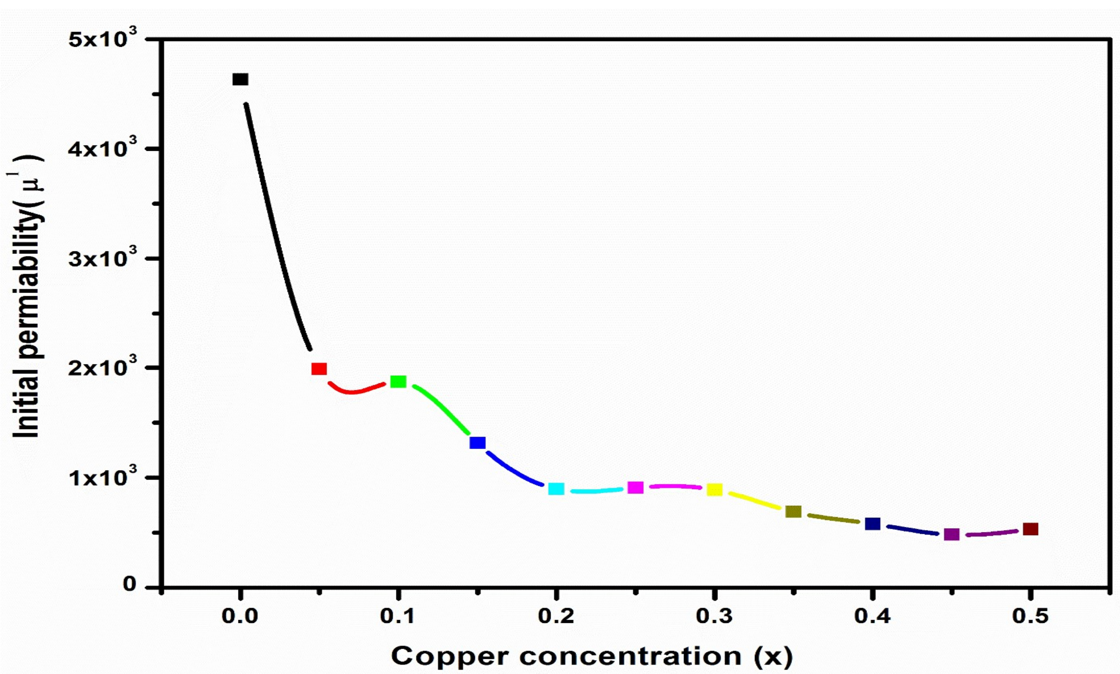

Figure 6: Variation of permeability with $Ni_{0.7-x}Cu_xZn_{0.3}Fe_2O_4$ ferrites system

Catalyst Research Volume 23, Issue 2, November 2023 Pp. 3452-3466

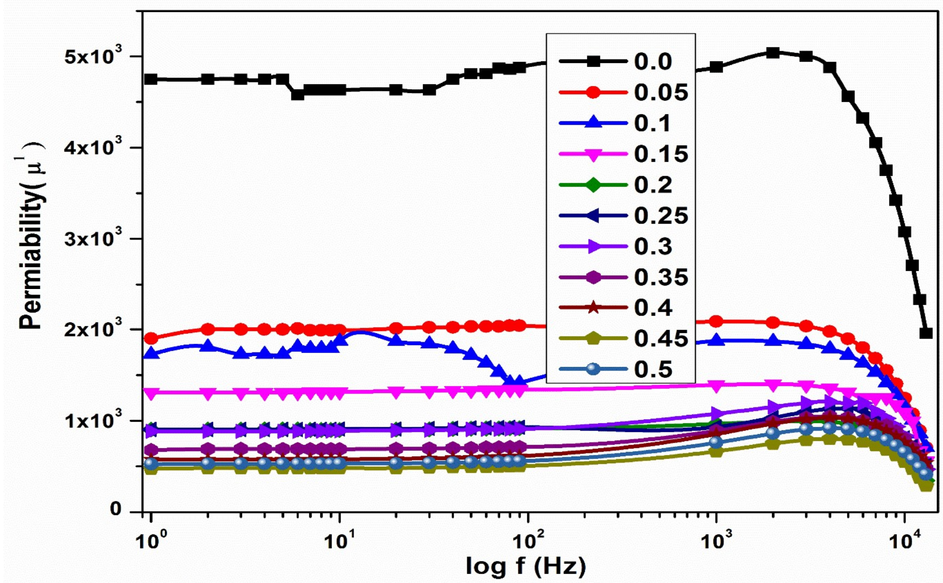

Figure 7: Permeability Vs. Frequency plots at room temperature for $Ni_{0.7-x}Cu_xZn_{0.3}Fe_2O_4$ ferrites system

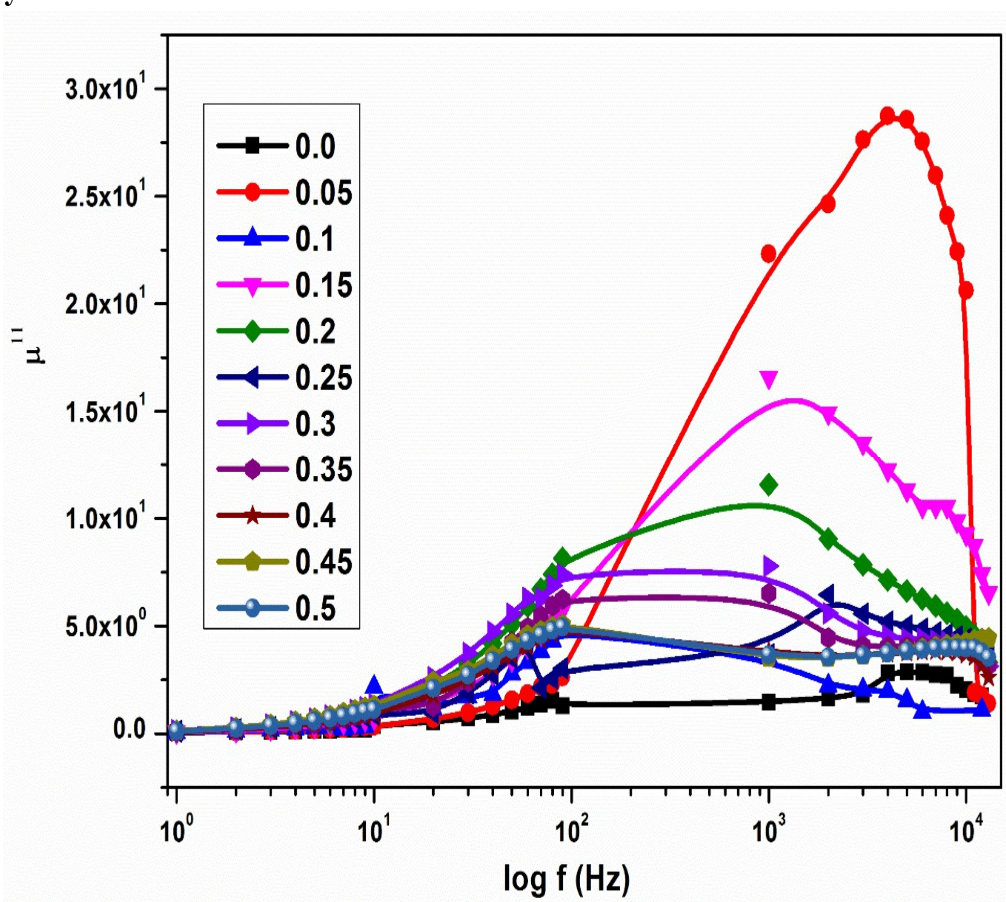

Figure 8: Variation of Complex permeability with log f for $Ni_{0.7-x}Cu_xZn_{0.3}Fe_2O_4$ ferrites system

Catalyst Research Volume 23, Issue 2, November 2023 Pp. 3452-3466

3.5 Dielectric constant

Dielectric constant (ε′) depends on frequency, decreases of dielectric constant (ε′) with increased frequency of $Ni_{0.7-x}Cu_xZn_{0.3}Fe_2O_4$ (x = 0.0, 0.05, 0.1, 0.15, 0.2, 0.25, 0.3, 0.35, 0.4, 0.45 and 0.5). A sudden decrease was observed at lower frequencies, and a gradual change at higher frequencies. The dielectric constant becomes negligible and independent at high frequency. This phenomenon is naturally observed in primary ferromagnetic materials and explained through a dielectric polarization process [27]. The electrical conductivity of ferrites happened because of the auto-adjust of an electron between the ions of the same atom where more than one vacancy state is distributed randomly in crystallographic lattice sites. Hole concentration is a characteristic of ferrites that depends on structure, temperature, and soaking time. Fe^{+2} is formed when hopping occurs between Fe atoms at +2 and +3 valance states. The charge transfer direction is the same approach as applying an electric field showing polarization in ferrites [28].

The concentrations of Fe^{2+}/Fe^{3+} ion pairs in the B-site can change the exchange value. As mentioned, the dielectric constant decreases with increasing frequency and reaches a saturation point. This trend is because, after a specific frequency of the external AC field, the charge transfer between Fe^{2+} and Fe^{3+} does not obey the alternating field.

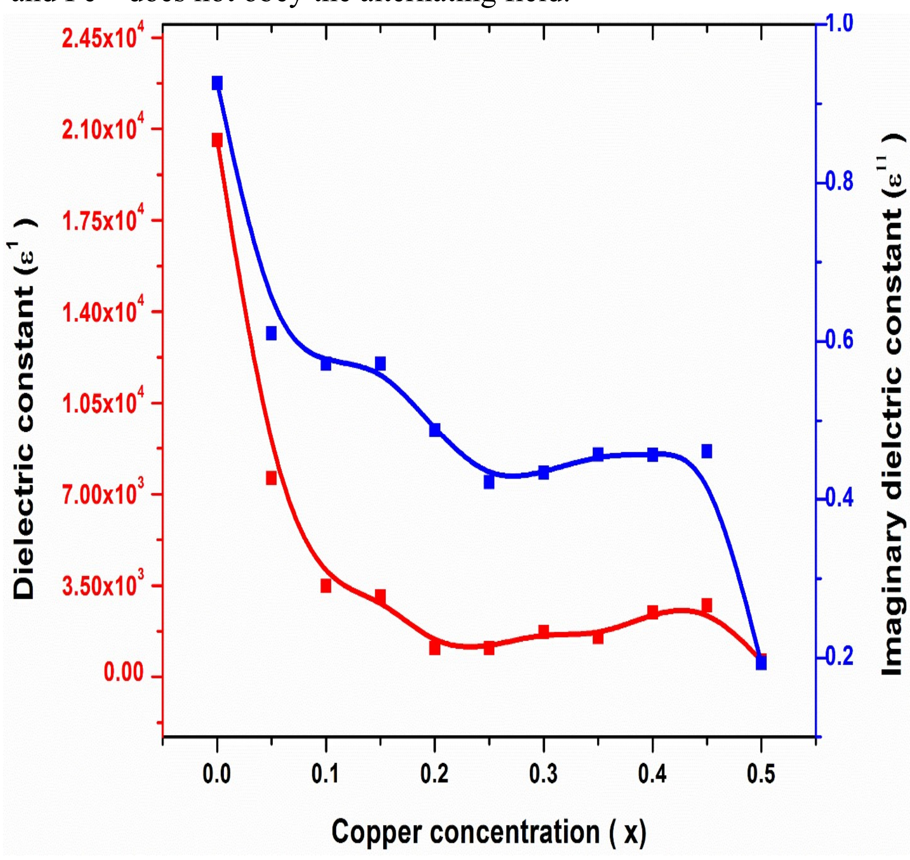

Figure 9: Variation of the ε′ & ε′′ at a frequency (10 kHz) for $Ni_{0.7-x}Cu_xZn_{0.3}Fe_2O_4$ ferrites system

From the literature, polycrystalline materials dielectric properties were altered by synthetic techniques, charge distribution, grain size, the Fe^{3+}/Fe^{2+} ions ratio, conductance, and sintering temperature in the same way ferrite samples behaved [29]. Ceramic fillers influence all composites' physical properties [30]. At a very high temperature, ferrites form as grains and are separated by air gaps or low conducting layers that act as heterogeneous dielectrics. A dielectric constant decreases and increases the Copper concentration in doping and saturated after $x = 0.30$, as shown in Figure 9. When copper replaces the nickel in B-sites provides Ni^{2+} and Ni^{3+} ions to balance the charge. These ion pairs, in turn, produce Fe^{2+} and Fe^{3+} ions at B-sites. Both these ionic pairs would create a hopping mechanism. The composition $x = 0.05$ showed the highest dielectric constant due to making more hopping pairs. The same is supported through DC resistivity measurements, where low resistivity has been noticed for the sample $x = 0.05$. The dielectric constant is higher in low frequency for ferrite materials [31]. According to the phenomenological theory of Koop and the interfacial polarization of Maxwell-Wagner [32].

The oxide grains are conducting, and their boundaries are resisting between the two layers of the ferrite dielectric. The expression relating dielectric constant and frequency is

$$\boldsymbol{\varepsilon''} = (\boldsymbol{\rho} - \boldsymbol{\rho'})(\boldsymbol{\varepsilon'} \times \boldsymbol{\omega})$$

where $\boldsymbol{\varepsilon'}$ and $\boldsymbol{\varepsilon''}$ are the real and imaginary parts of the dielectric constant, $\boldsymbol{\rho}$ and $\boldsymbol{\rho'}$ are the AC and DC conductivities, and $\omega = 2\pi f$ is the angular frequency with f, the frequency. The dielectric constant is steady till 13 MHz.

3.6 Dielectric loss

The tangent loss is the dissipation of the electromagnetism energy from the dielectric material. Figure 10 shows the value of frequency-dependent dielectric loss varied with $Ni_{0.7-x}Cu_xZn_{0.3}Fe_2O_4$ (x = 0.0, 0.05, 0.1, 0.15, 0.2, 0.25, 0.3, 0.35, 0.4, 0.45 and 0.5). Dielectric loss decreases with increasing log frequency, and loss rises with the copper substituent [33]. This may be attributed to the increased conduction mechanism enhancing the resultant sample by decreasing the resistivity. The dielectric constant is found to be similar to that of dielectric loss. The humps at 100 kHz show the correlated conducting and dielectric behavior due to the divalent and trivalent ions at the B site [34].

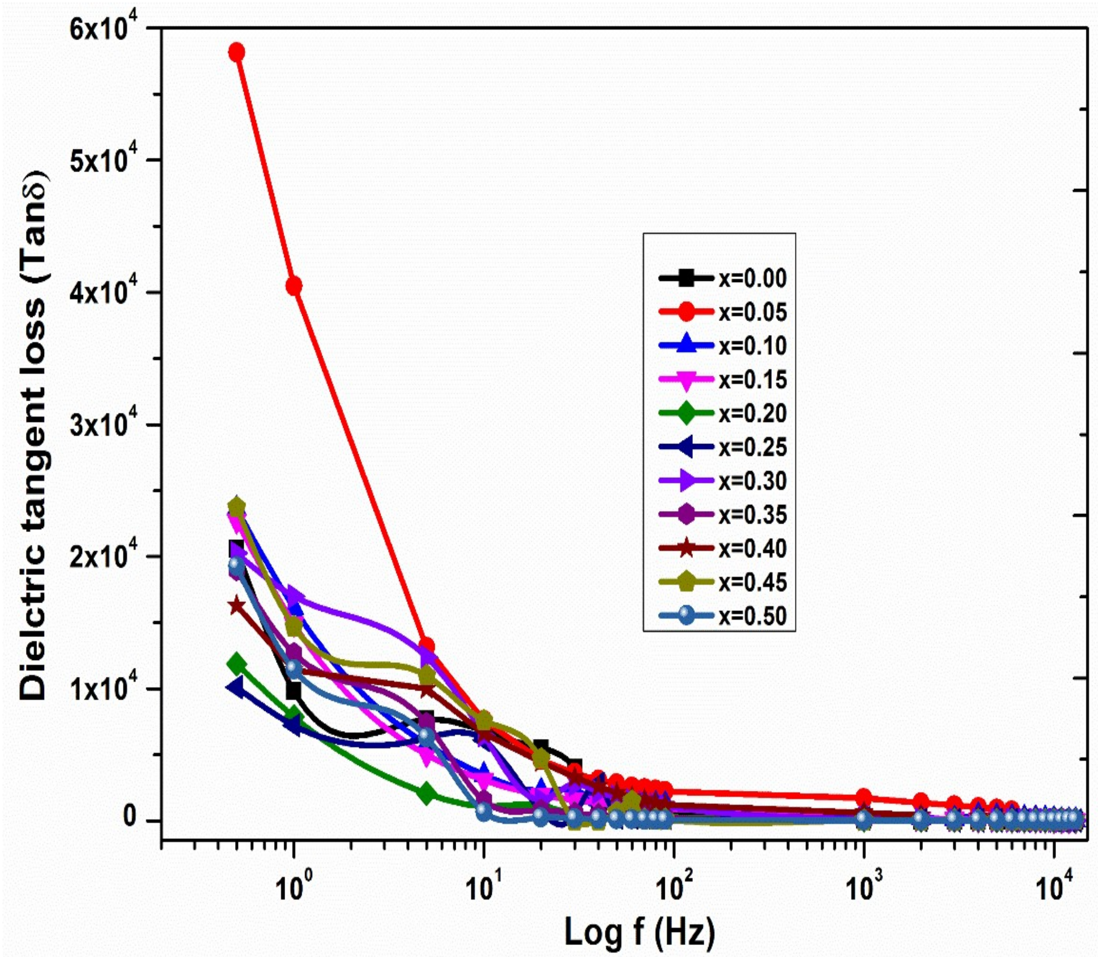

Figure 10: Graph between frequency-dependent dielectric loss Vs. frequency for $Ni_{0.7-x}Cu_xZn_{0.3}Fe_2O_4$ ferrites system

4. Conclusions

$Ni_{0.7-x}Cu_xZn_{0.3}Fe_2O_4$ (x = 0.0, 0.05, 0.1, 0.15, 0.2, 0.25, 0.3, 0.35, 0.4, 0.45 and 0.5) ferrite particles were prepared with solid-state reaction method. Their structure was a single-phase spinel with increasing lattice parameters for increasing 'x'. Their morphology shows the randomly oriented uniform micro grains. The initial permeability decreases gradually with increasing 'x' due to the diamagnetic behavior of copper. Consequently, the saturation magnetization decreases. The grain size increases with increasing copper content during the initial permeability decrease. The values of initial permeability remain constant with increasing the frequency up to 10 MHz due to domain wall motion in low frequencies. Beyond 10 MHz, the initial permeability increases, resonance due to domain wall displacement is noticed up to 13 MHz and then falls.

References

1. A. Nakano, S. Saito, and T. Nomura, “Composite Multilayer Parts” US Patent5476728, (1995).
2. P.K. Roy, J. Bera, `J. Magn. Magn.Mater.**321**, 247 (2009).

3. H. Su, H.W. Zhang, X.L. Tang, L.J. Jia, Q.Y. Wen, Mater. Sci. Eng. B**129** 172–175 (2006).

4. C.L. Miao, J. Zhou, X.M. Cui, X.H. Wang, Z.X. Yue, L.T. Li, Mater. Sci. Eng. B **127**, 1-5 (2006).

5. J.-Y. Hsu, W.-S.Ko, H.-D. Shem, C.-J.Chen, IEE Trans. Magn, **30** (6) 4875 (1994).

6. T. Nakumura, J. Magn. Mag. Mater. **168**(3), 285 (1997).

7. S. C. Byeon, H.-J.Je, K.S. Hong, Jpn.J. Appl. Phys. **36**, 5103 (1997).

8. S. Modak, M. Ammar, F. Mazaleyrat, S. Das, and P. K. Chakrabarti, J. All. Compd.**473**(1-2), 15 (2009).

9. Hsu, J.Y., Ko, W.S., Chen, C.J. IEEE Trans. **31**: 3994-3996 (1995).

10. P. Himakar, N. Murali, D. Parajuli, V. Veeraiah, K. Samatha, Tulu Wegayehu Mammo, Khalid Mujasam Batoo, Muhammad Hadi, Emad H. Raslan, and Syed Farooq Adil, Journal of Electronic Materials (2021): 1-9.

11. Mallapur, M.M.; Shaikh, P.A.; Kambale, R.C.; Jamadar, H.V.; Mahamuni, P.U.; Chougule, B.K. Journal of Alloys and Compounds 2009, 479, 797-802.

12. Knyazev, A.V.; Zakharchuk, I.; Lähderanta, E.; Baidakov, K.V.; Knyazeva, S.S.; Ladenkov, I.V. Journal of Magnetism and Magnetic Materials 2017, 435, 9-14.

13. Saohoo. R.F. Engle wood cliffs. N.J., Prentice Hall 6 (1960).

14. D.L. Fresh, Proc. IRE **49**, 1303 (1956).

15. Yu S, Wu G, Gu X, Wang J, Wang Y, Gao H, et al. Colloids Surf, 103 (2013) 15–22.

16. Tejabhiram Y, Pradeep R, Helen AT, Gopalakrishnan C, Ramasamy C. Mater Res Bull 2014;60:778–82.

17. Jha DK, Shameem M, Patel AB, Kostka A, Schneider P, Deb AEP. Mater Lett 2013;95:186–9.

18. Kenouche S, Larionova J, Bezzi N, Guari Y, Bertin N, Zanca M, et al. Powder Technol 2014;255:60–5.

19. A. Ramakrishna, N. Murali, Tulu Wegayehu Mammo, K. Samatha, V. Veeraiah, Phys. B: Condens. Matter 534 (2018)134-140.

20. Min Ji Hyun, Woo Mi-Kyung, Yoon Ha Young, Jang Jin Woo, Wu Jun Hua, Lim Chae-Seung, et al. Anal Biochem 2014;447:114–8.

21. Drmota A, Koselj J, Drofenik M, Znidarsic A. J Magn Magn Mater 2012;324:1225–9.

22. P.K. Roy, J. Bera, J. Mag. Mag. Mater.**321**, 247–251 (2009).

23. R. Lebourgeois, C. Le. Fur, M. Labeyrie, M. Pate, J. P. Ganne. J. Mag. Materials, 160, 329-332 (1996).

24. N. Murali, S. J. Margarette, G. Pavan Kumar, B. Sailaja, S. Yonatan Mulushoa, P. Himakar, B. Kishore Babu, and V. Veeraiah, Physica B: Condensed Matter 522 (2017): 1-6.

25. M.R. Anantharaman, S. Sindhu, S. Jagatheesan, K.A. Malini and Philip Kurian, J. Phys. D: Appl. Phy.**32**, 1801-1810 (1999).

26. Yadoji P, Ramesh P, Dinesh A, Roy R. Mat. Sci. Eng. B**98**, 269-278 (2003).

27. S.A. Mazen, M.H. Abdallah, M.A EIghandoor and H.A Hashem*, Phys. Stat. Sol*. (a) **144**,461-470 (1994).

28. Ramakrishna, A., Murali, N., Mammo, T.W., Samatha, K. and Veeraiah, V., Physica B: Condensed Matter 534 (2018) 134-140.

29. Raju, G., Murali, N., Prasad, M.S.N.A., Suresh, B., Babu, D.A., Kiran, M.G., Ramakrishna, A., Wegayehu, M.T. and Babu, B.K., Materials Science for Energy Technologies 2 (2019) 78-82.

30. Mercy, S.J., Murali, N., Ramakrishna, A., Ramakrishna, Y., Veeraiah, V. and Samatha, K., Applied Physics A 126 (2020) 1-13.

31. Ramakrishna, A., Murali, N., Margarette, S.J., Samatha, K. and Veeraiah, V., Physica B: Condensed Matter 530 (2018) 251-257.

32. K. Chandramouli, P. Anantha Rao, B. Suryanarayana, Vemuri Raghavendra, Shaik Jesus Mercy, D. Parajuli, Paulos Taddesse, S. Yonatan Mulushoa, Tulu Wegayehu Mammo, and N. Murali, Journal of Materials Science: Materials in Electronics (2021): 1-9.

33. P. Himakar, K. Jayadev, D. Parajuli, N. Murali, Paulos Taddesse, S. Yonatan Mulushoa, Tulu Wegayehu Mammo, B. Kishore Babu, V. Veeraiah, and K. Samatha, Applied Physics A 127, no. 5 (2021): 1-10.

34. K, Chandramouli, B. Suryanarayana, P. V. S. K. Phanidhar Varma, Vemuri Raghavendra, K. A. Emmanuel, Paulos Taddesse, N. Murali, Tulu Wegayehu Mammo, and D. Parajuli, Results in Physics 24 (2021): 104117.